Side-Chain Crystallization in Alkyl-Substituted Semiflexible Polymers

J. L. Lee, E. M. Pearce, and T. K. Kwei*

Department of Chemical Engineering, Chemistry, and Materials Science, Polytechnic University, Six Metrotech Center, Brooklyn, New York 11201

Received March 24, 1997; Revised Manuscript Received June 23, 1997[⊗]

ABSTRACT: A series of comblike semiflexible polymers, in which the alkyl side chains were located nonsymmetrically on the ring, were synthesized by reacting hydroxypropylcellulose (HPC) with hexyl, octyl, dodecyl, and octadecyl isocyanates. Side-chain melting was observed in DSC experiments for polymers with 12 and 18 carbons in the pendant groups (C12HPC and C18HPC). Wide-angle X-ray (WAXS) studies indicated that the alkyl groups in C12HPC crystallized in a form similar to the β_T crystal of hydrocarbons but multiple crystalline forms coexisted in C18HPC. However, reorganization of the alkyl side chains was observed as the polymers underwent thermal transitions. A better packing of the alkyl side chains could be induced by shearing the samples in the molten state followed immediately by slow cooling. Quenching and annealing studies suggested that side-chain crystallization and reorganization could influence the packing of the semiflexible backbone. The interplay between the main chain and the side chain in order development is described.

Introduction

Comb-type polymers containing long alkyl side groups were studied as early as 1964.[1] Differential scanning calorimetry (DSC) and wide-angle X-ray scattering (WAXS) investigations on poly(*n*-alkyl acrylates),[2,3] poly(*n*-alkyl methacrylates),[4,5] poly(acrylamides), and their copolymers[5] suggested that side-chain crystallization took place when its length exceeded eight carbon atoms. In spite of the different chemical structures investigated in these studies, the flexible main chains seemed to be able to adapt themselves to side-chain organization.

Side-chain crystallization was also observed in alkyl-substituted rigid polymers such as aromatic polyesters,[6−10] polyamides,[11−14] polyimides,[8] polythiophenes,[15−17] and polyanilines[18] when the number of carbon atoms in the side groups (*n*) was 12 or higher. The rigid backbone seemed to exert a strong influence on side-chain crystallization. In addition, the melting temperature of the side chains (T_s) was affected not only by the length of the alkyl chains but also by the number of substituents.

The primary purpose of this study is to investigate side-chain crystallization in a semiflexible polymer and to investigate how it is influenced by the thermal and mechanical histories of the sample. The polymer of our choice was hydroxypropylcellulose (HPC). The hydroxyl groups on the anhydroglucose unit of HPC enable facile reactions and modifications of the structure to be accomplished without a major synthetic effort. By reacting all the hydroxyl groups, we can arrive at a structure in which three long substituents are located nonsymmetrically on the ring. Whereas side-chain order in both flexible and rigid polymers (with one exception) was thought to involve the interdigitation of the alkyl groups from different chains, the alkyl side chains emanating from the C2 and C3 positions in HPC are so close to each other that there would be insufficient space to accommodate another incoming alkyl chain from the opposite direction. Consequently, the arrangement of side chains would be different from the majority of the literature examples. The second objective of our research, therefore, is to study the interplay between the semiflexible main chain and the side chain in order development in the solid state.

Experimental Section

Reagents. All the chemicals used in this study were purchased from Aldrich Chemical Co. and were used as received if not specified otherwise. Hexyl and octyl isocyanates were purified by distillation at 30 °C/0.8 mmHg and 55 °C/1 mmHg, respectively. Dodecyl and octadecyl isocyanates were filtrated by 0.45-μm filters. HPC (reported $M_W = 10\,000$, $M_w/M_n = 2.5$) was dried at 55 °C under vacuum for 12 h to remove absorbed moisture before use. The degree of substitution (DS) and molar substitution (MS) were estimated to be 2.8 and 4.2, respectively, by ^{13}C NMR spectra.[19]

Synthesis of C*n*HPC's. HPC was dissolved in anhydrous pyridine and stirred for 2 h to form a homogeneous solution. One gram of 5% catalyst solution (dibutyltin dilaurate in anhydrous pyridine) was added to the solution. Hexyl, octyl, dodecyl, or octadecyl isocyanates were then added to the solution at a molar ratio of 3.6/1 (RNCO/HPC) and were allowed to react at 45 °C for 12 h. The synthetic procedures were represented in Scheme 1. C*n*HPC's were precipitated in water, and the products, except for C18HPC, were sticky. Liquid nitrogen was employed to solidify the precipitates which were then ground into fine powders. The polymer powder was finally rinsed by small amounts of acetone followed by vacuum drying for at least 12 h. The resulting white powders were obtained at yields of about 80%.

Infrared Spectra. A Perkin-Elmer PE1600 Fourier transform infrared (FT-IR) spectrometer was used to identify the functional groups in HPC and its derivatives. C*n*HPC's were dissolved in $CHCl_3$, and the solution was then cast on a NaCl pellet followed by slow evaporation of the solvent.

Nuclear Magnetic Resonance (NMR) Spectra. A General Electric GN-300 Fourier transform nuclear magnetic resonance spectrometer (FT-NMR) operating at 300 MHz was used to determine the structures of HPC and its derivatives in $CDCl_3$.

Differential Scanning Calorimetry (DSC). Two modes of operation for the DSC studies were carried out on a TA 2920 Modulated DSC. In the standard mode, a rate of 10 °C/min was used in the heating/cooling cycle experiments. In the modulated mode, the underlined heating rate and modulation amplitude were selected so that the samples were continuously heated during the run. The modulation frequency was chosen to have four cycles or more in the interested transition temperature range based on the thermograms from the standard mode to ensure good resolution and separation of

[⊗] Abstract published in *Advance ACS Abstracts,* October 1, 1997.

S0024-9297(97)00404-X CCC: $14.00

Scheme 1. Synthesis of C*n*HPC's.

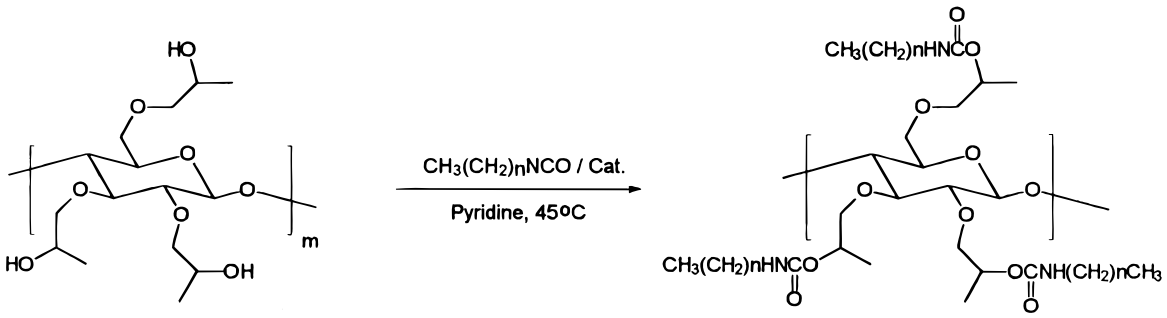

Table 1. Elemental Analyses of HPC and Its Derivatives

	calcd (MS = 4.2)			calcd (MS = 3.0)			found		
	C%	H%	N%	C%	H%	N%	C%	H%	N%
HPC	54.97	8.97		53.57	8.33		53.48	8.72	
C6HPC	60.30	9.57	5.33	60.25	9.34	5.86	61.03	9.81	6.11
C8HPC	62.75	10.02	4.82	62.92	9.86	5.24	64.01	10.34	5.37
C12HPC	66.46	10.71	4.04	66.87	10.63	4.33	68.48	11.45	4.63
C18HPC	70.22	11.41	3.25	70.76	11.38	3.44	71.73	11.90	3.55

signals. For most determinations, a heating rate of 5 °C/min with ±0.75 °C/min modulation was used.

Wide-Angle X-ray Scattering (WAXS). X-ray diffraction patterns were obtained from a Philips 3100 X-ray generator with a Philips APD-3720 diffractometer, in which the high-intensity monochromatic Cu Kα radiation with an average wavelength 1.5418 Å was generated. In addition to the pulverized powders, the bulk samples were melted on a hot stage (Melttler FP82) and sheared manually, followed by various cooling rates to form homogeneous films for the X-ray experiments.

Results

Elemental Analyses. The results of the elemental analysis are listed in Table 1. When the experimental results are compared with the calculated values based on a MS of 4.2 estimated from NMR data, the experimental nitrogen percentages are always higher by 0.3−0.6%. On the other hand, if the MS is assumed to be 3.0, the two sets of values are in reasonable agreement. We are inclined to think that the correct value of MS is closer to 3 than to 4.2 since there are significant uncertainties in the NMR peak area measurements.

FT-IR. The broad absorption at 3500 cm^{-1} in HPC is absent in all derivatives and replaced by the absorption at 3340 cm^{-1}, which is assigned to N−H stretching. For C*n*HPC's, the absorption peaks at 1700 cm^{-1} and the shoulder at 1730 cm^{-1} are associated with the hydrogen-bonded and free C═O stretching vibrations, respectively, in the urethane linkage.[20] The peaks at 1534 cm^{-1} (amide II) and 1230 cm^{-1} (C−N stretching) unambiguously confirm the formation of urethane linkages.

^{13}C NMR. Figure 1 shows the ^{13}C NMR spectra of HPC in D_2O and C8HPC in $CDCl_3$, respectively. The peaks at 104.7 and 69.4 ppm are characteristic of C1 and substituted C6, respectively. Ring carbons and the C7's fall in the range 75−85 ppm. Peaks for the terminal (E) and inner methyl carbons (I) are located at 21.3 and 18.9 ppm, respectively. The formation of the urethane linkage was evident in the ^{13}C NMR spectra. A resolved doublet at 156 and 158 ppm corresponded to the free and bonded carbonyl carbons, respectively. In addition, another doublet near 40 ppm arose from the methylene carbon next to the N atom in the alkyl portion.

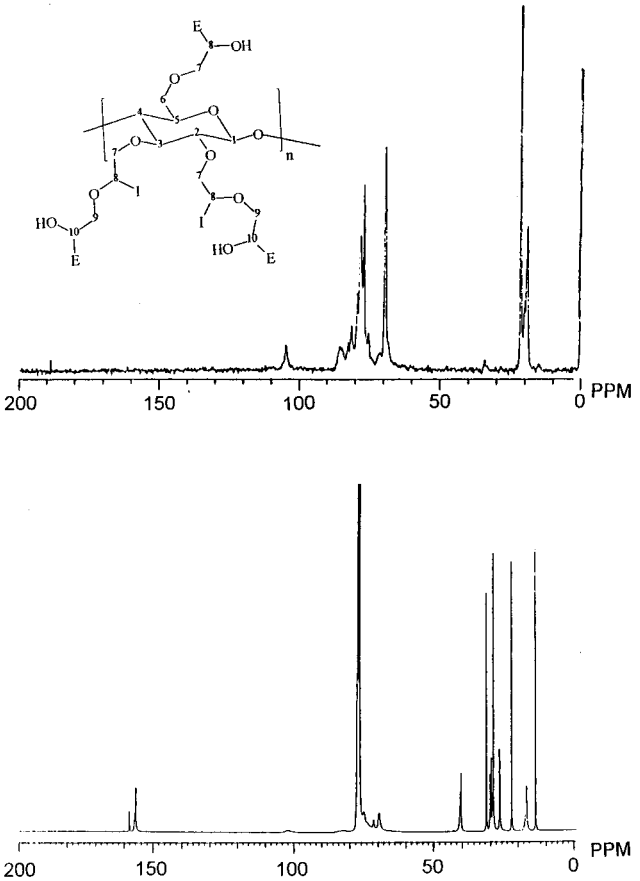

Figure 1. ^{13}C NMR spectra of HPC in D_2O (top) and C8HPC in $CDCl_3$ (bottom) at room temperature.

Glass Transition Temperature (T_g). HPC showed a broad glass transition around 50 °C and a melting peak at 195 °C in the DSC scan, followed by degradation above 220 °C. The T_g's of the as-made C6HPC and C8HPC were located at −8 and −7 °C, respectively, in conventional DSC experiments, but the transitions for C12HPC and C18HPC could not be detected. After quenching from the molten state, C6HPC and C8HPC exhibited glass transitions at −19 and −23 °C, respectively, in the second heating scans with a heating rate of 10 °C/min. However, the glass transition temperatures were again not observed for quenched C12HPC and

Table 2. Thermal Transitions of C*n*HPC's

	T_g, °C			T_s, °C		T_2, °C		T_i, °C	
	first heat	second heat	MDSC	first heat	second heat	first heat	second heat	first heat	second heat
C6HPC	−8	−19	−4					70	68
C8HPC	−7	−23	−9					90	82
C12HPC			−16	45		73	73	106	106
C18HPC				52/58	56	73	73	115	115

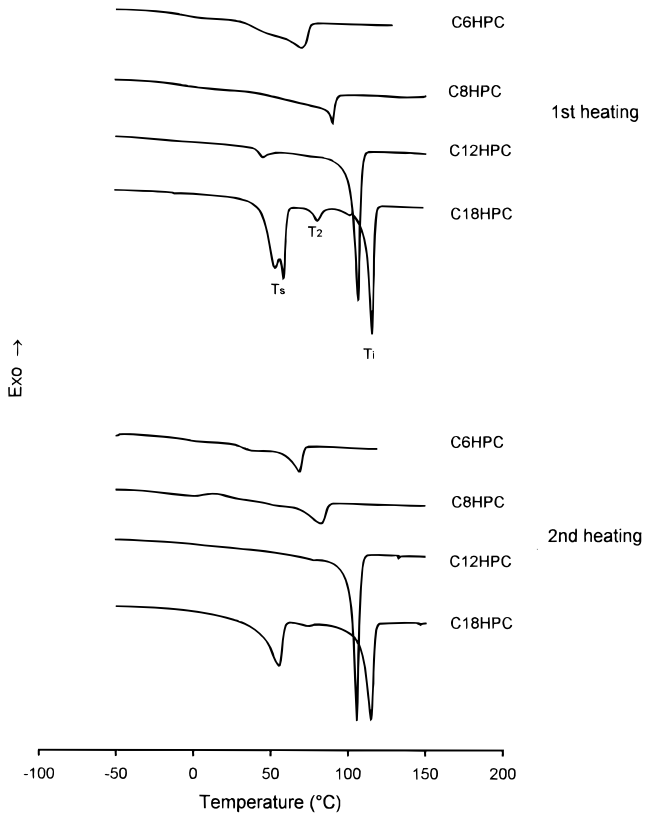

Figure 2. DSC traces of C*n*HPC's at a rate of 10 °C/min. First heating scans of the as-made samples (top) and the second heating after −10 °C/min cooling (bottom).

C18HPC. Modulated differential scanning calorimetry (MDSC) was then employed. The results of both methods of measurements are complied in Table 2.

DSC Studies of CnHPC's. The first heating scan of the as-prepared C6HPC exhibited, aside from a step change in specific heat at −8 °C, a broad melting transition with peak temperature at 70 °C, Figure 2. Crystallization from the melt occurred at 39 °C when the sample was cooled at a rate of 10 °C/min. Faster cooling (ca. −20 °C/min) from the molten state resulted in the observation of a cold crystallization exotherm at 7 °C in the second heating scan, after the T_g at −19 °C was traversed. C8HPC responded similarly to the heating/cooling cycle. A melting transition was seen at 90 °C, and upon subsequent cooling, the crystallization exotherm was located at 60 °C. Since neither C6HPC or C8HPC exhibited side-chain melting in their respective DSC scans, these results will not be analyzed further in this paper.

The as-prepared C12HPC and C18HPC samples behaved differently under the same experimental conditions. Three endothermic peaks, T_1, T_2, and T_3, were observed for each polymer in the first heating scan. C12HPC unfolded two first-order transitions at 45 °C (T_1) and 106 °C (T_3), as well as a very shallow endothermic event around 73 °C (T_2). The location of T_1 suggests itself as the side-chain melting point (T_s), and

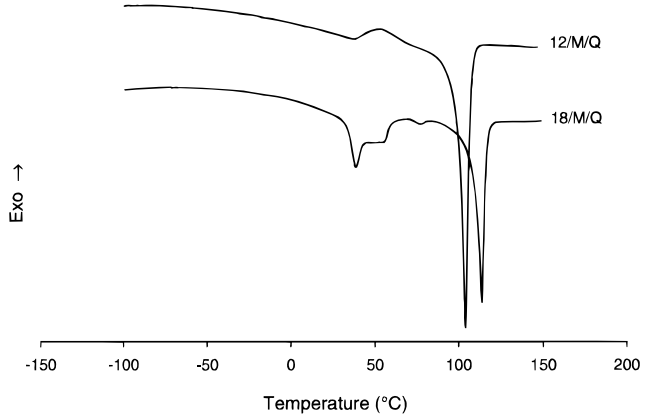

Figure 3. DSC heating traces (10 °C/min) of the quenched C12HPC and C18HPC (bottom).

the sharp endotherm at 106 °C (T_3) is the isotropic transition temperature (T_i) confirmed by polarized optical microscopy. C18HPC displayed a sharp endotherm at 115 °C (T_3) due to isotropization, along with a double-melting peak (T_s) at 52 and 58 °C. The locations of T_2 and T_i remained essentially the same in the second heating scan, but the T_s endotherm changed significantly. No transition was observed in the T_s region in the second heating scan of C12HPC even when the sample had been cooled very slowly from the melt. On the other hand, the double-melting behavior of T_s in C18HPC reshaped into a single peak at 56 °C with an associated ΔH_s about half the value found in the first run. The thermal event at T_2 is not understood at present. The thermal transitions of each sample are summarized in Table 2.

In order to gain insight into the T_s transition, C12HPC and C18HPC were quenched in liquid nitrogen from the molten state. Surprisingly, the DSC heating scan of quenched C12HPC showed a melting endotherm at 40 °C which was only seen in the first heating scan of the as-made sample. On the other hand, the quenched C18HPC revealed a double-melting peack at 38 and 51 °C (Figure 3). Another set of samples were annealed at various temperatures, followed by different cooling processes. After C12HPC had been kept for 12 h at an annealing temperature (T_a) of 65 °C, between T_s and T_i, and then cooled at −10 °C/min, the sample exhibited a tiny but visible endotherm at ca. 40 °C in addition to the major peak at 106 °C (T_i). Annealing the sample in the molten state followed by cooling again at 10 °C/min caused the disappearance of the T_s peak. When C18HPC was subjected to the same annealing procedure at a T_a of 65 °C and then cooled at a rate of 10 °C/min, the subsequent heating scan displayed a sharp endothermic peak at 59 °C with a shoulder at 53 °C. When cooled at a faster rate (ca. 20 °C/min), the same annealed sample showed a broader peak at 56 °C. It should be pointed out as a reminder that this endotherm was observed previously when C18HPC was cooled from the isotropic state at a rate of 10 °C/min. Figure 4 shows the DSC thermograms of the annealed C12HPC and C18HPC cooled at different rates. The peak tem-

Table 3. ΔH_s's and ΔH_i's of Thermally Conditioned C12HPC and C18HPC

	sample	cooled from	cooling rate, °C/min	T_s, °C	ΔH_s, J/g	T_i, °C	ΔH_i, J/g
as-made	C18HPC			52, 58	96.2[a]	115	50.1
18/M/-10	C18HPC	molten state	−10	56	51.4	115	49.0
18/M/-20	C18HPC	molten state	−20	55	48.3	115	49.0
18/M/Q	C18HPC	molten state	quenching	38, 51[c]	53.1[a]	114	41.0
18/A/−1	C18HPC	65 °C	−1	60[b]	75.8	115	43.6
18/A/−10	C18HPC	65 °C	−10	59[b]	71.3	115	48.8
18/A/−20	C18HPC	65 °C	−20	55	56.1	115	46.7
as-made	C12HPC			45	15.7	106	73.5
12/M/−10	C12HPC	molten state	−10	N/A	N/A	106	68.4
12/M/−20	C12HPC	molten state	−20	N/A	N/A	106	70.1
12/M/Q	C12HPC	molten state	quenching	36[c]	23.4	104	60.4
12/A/−1	C12HPC	65 °C	−1	41	6.7	106	66.9
12/A/−10	C12HPC	65 °C	−10	40	4.6	106	67.6
12/A/−20	C12HPC	65 °C	−20	40	2.9	106	67.1

[a] ΔH_s is the sum of transition enthalpy of the two overlapped peaks; note that the ΔH_s value has been normalized by the weight of the alkyl side chain. [b] A shoulder at 53 °C in addition to the side-chain melting peak. [c] Broad endotherm.

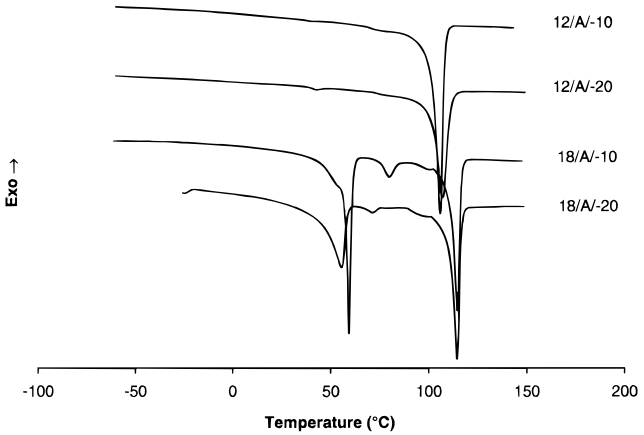

Figure 4. DSC heating traces (10 °C/min) of the annealed C12HPC and C18HPC cooled at −10 or −20 °C/min.

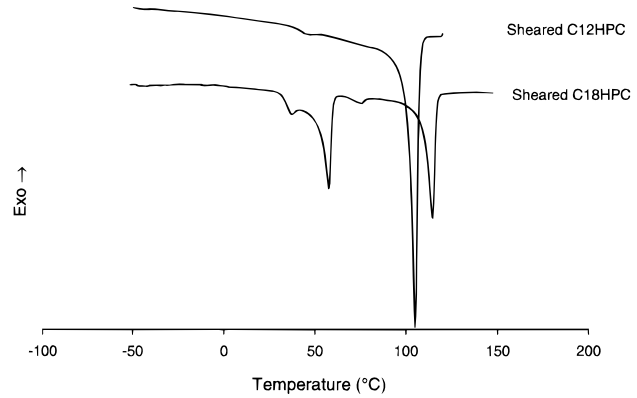

Figure 5. DSC heating traces (10 °C/min) of the sheared C12HPC (top) and C18HPC (bottom).

peratures of the endotherms and the associated enthalpy changes are complied in Table 3, in which the ΔH_s value is normalized by the weight of the alkyl side chain.

To study the effect of shear, DSC experiments of the sheared samples were carried out and the thermograms are shown in Figure 5. For C12HPC, the high-temperature (T_i) endotherm occurred at almost the same temperature as in the unsheared sample. However, the low temperature (T_s) endotherm which could not be seen in the second heating scan of the unsheared sample now appeared at 45 °C. Reheating the sample to the molten state caused the thus-generated peak at 45 °C to disappear in the subsequent scan, but T_i did not change. For the sheared C18HPC, the T_s endotherm split into two peaks, a small one at 37 °C and a larger one at 57 °C. Reheating the sheared sample to the molten state followed by either slow or fast cooling brought the peak back to 56 °C, the same temperature found in the second run of the as-made sample.

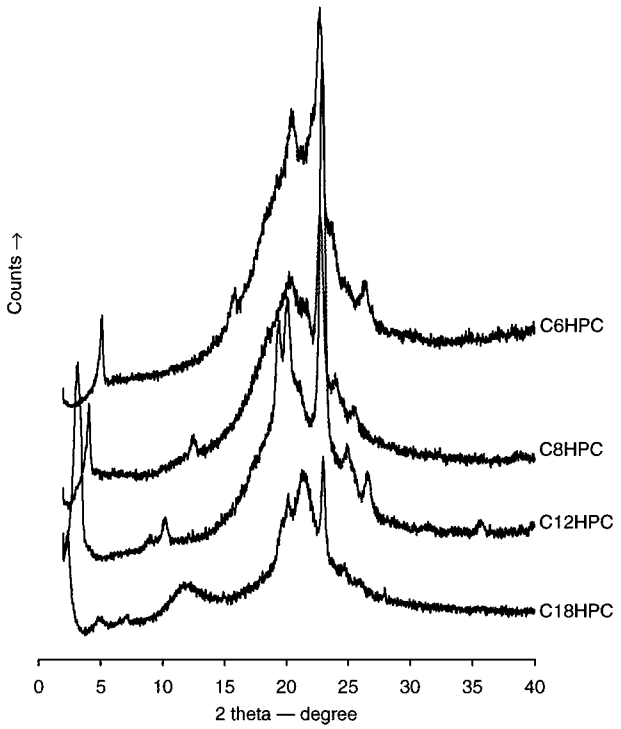

Figure 6. WAXS profiles of the as-made C*n*HPC's.

Wide-Angle X-ray Scattering. Figure 6 shows the WAXS profiles of the as-made powder HPC derivatives. All samples displayed the odd-numbered diffractions in the low-angle region, except for C18HP, which showed a pattern of the well-defined layered structure. The low-angle data and their interpretation in relation to the layered structure as well as polymer morphology will be addressed in a separate publication. Only the diffraction results in the region $2\theta = 16-28°$ will be discussed here. The diffraction peak at $d = 3.9$ Å was predominant in all cases. C6HPC and C8HPC exhibited similar patterns in this region, with weak diffraction peaks at 4.4, 3.7 and 3.5 Å. Both C12HPC and C18HPC showed multiple diffraction peaks in the region of 4.6−3.4 Å. However, C18HPC exhibited a distinct peak at 4.2 Å and a shoulder at 4.5 Å relative to the peak at 4.4 Å. The *d* spacings of the corresponding diffraction peaks of each sample are listed in Table 4.

Table 4. WAXS Diffractions (Å) of the As-Made C*n*HPC's

	low-angle region				wide-angle region				
C18HPC	37.1	18.2	12.4	7.4	4.5[a]/4.4	4.2	3.9	3.6	3.4
C12HPC	27.6	8.7			4.6	4.4	3.9	3.6	3.4
C8HPC	21.7	7.1			4.4/4.1[a]	3.9	3.7	3.5	
C6HPC	17.2	5.6			4.3	3.9	3.7	3.6	3.4

[a] Shoulder to the neighboring peak.

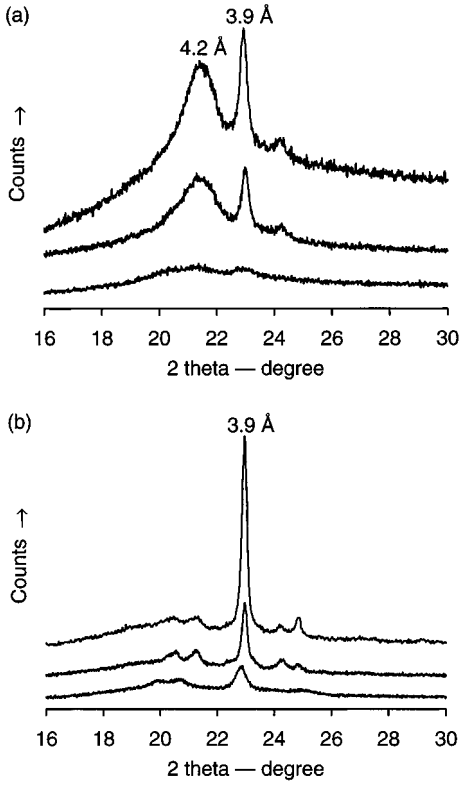

Figure 7. WAXS profiles of the sheared (a) C18HPC and (b) C12HPC. The three curves in each set are the diffractions with processes 1, 2, and 3 (from top to bottom).

Table 5. Diffractions of Sheared C18HPC and C12HPC

	diffractions, (Å)				
18-I[a]	4.2	3.9	3.7		
18-II	4.2	3.9	3.7		
18-III	4.2	3.9			
12-I	4.4	4.2	3.9	3.7	3.6
12-II	4.3	4.2	3.9	3.7	3.6
12-III	4.5	4.3	3.9	3.6	

[a] I: process 1, slow cooling without annealing. II: process 2, slow cooling after 10 min of annealing. III: process 3, fast cooling (ca. −50 °C/min) after 10 min of annealing.

To compare with DSC experiments, the sheared C12HPC and C18HPC samples were cooled from the molten state by three different processes: (1) slow cooling immediately after being sheared, (2) annealing in the molten state for 10 min after shearing followed by slow cooling, and (3) annealing in the molten state after shearing followed by fast cooling at a rate of ca. 50 °C/min. Processes 2 and 3 were designed to reveal the effects of cooling rate when the shear effect was nullified by annealing in the molten state.[21] The diffractions in the wide-angle region are shown in Figure 7, and the results are compiled in Table 5.

Regardless of the various cooling processes used, the diffraction at 3.9 Å was predominant in all C12HPC samples. Slow cooling (with and without annealing) retained the multiple peaks in the 3.6−4.4-Å region. Fast cooling from the molten state of the annealed C12HPC resulted in the disappearance of the peak at 3.7 Å. Shearing in the melt also influenced the diffraction pattern of C18HPC. For the sample subjected to process 1, the diffraction at 4.2 Å, had been reinforced in relation to the previously predominant peak at 3.9 Å. Reheating the above sample to the isotropic state for a period of time followed by slow cooling (process 2) resulted in a shoulder at 4.4 Å next to the major peak at 4.2 Å, which now had a reduced peak intensity. Fast cooling of the annealed sample (process 3), however, led to two amorphous halos at 4.2 and 3.9 Å, respectively.

Discussion

(a) As-Prepared Samples. As described in the Introduction, the length (n) required for the crystallization of alkyl side chains was 8 or higher for flexible polymers and 12 or higher for rigid polymers. In this series of HPC derivatives, a side-chain melting endotherm was not observed in C6HPC and C8HPC but was observed in C12HPC and C18HPC.

The as-made C12HPC sample displayed an endotherm at 45 °C with a ΔH_s=15.7 J/g, due to the melting of the side-chain crystals. This melting endotherm was not seen in subsequent heating/cooling scans after the sample was heated to the molten state. Similar observations were found in the literature, for example, in Wegner's study of dialkyl-substituted aromatic polyesters, with $n = 6-10$.[9] "Unstable" crystals of the as-made sample, which were only observed in the DSC first heating scan, were also reported for main-chain liquid-crystalline polymers containing long methylene sequences as spacers.[22] In C18HPC, the first heating scan of the as-made sample showed a double-melting peak at 52 and 58 °C with a total ΔH_s of 96.2 J/g. This double-melting behavior might be indicative of nonuniform or multiple modifications of side-chain crystal formation since the sample was precipitated from a nonsolvent.

Before we engage in the discussion of X-ray diffraction results, it is useful to cite the crystal structures of n-paraffins as reference points for comparison. The α-hexagonal (α_H) modification existed in n-paraffins with $9 < n < 43$ when n was odd or $22 < n < 44$ when n was even.[23] The lower energy β-orthorhombic (β_O) crystalline form was found in the n-paraffins with $n > 9$ when n was odd or $n > 40$ when n was even. For $n < 24$, β-triclinic (β_T) was commonly observed in the even series of n-paraffins, even when n was as low as 4, 6, and 8. On the other hand, β-monoclinic (β_M) prevailed in the even series when n was greater than 26. The X-ray diffrations for each n-paraffin crystalline modification are as following; α_H, 4.2, 2.4, and 2.1 Å; β_T, 4.5, 3.8, and 3.6 Å; β_O, 3.7 Å.[24]

Side-chain order was evident in the wide angle region of the WAXS profiles, based on n-paraffin crystal structures. For C12HPC, the side-chain diffraction pattern (4.6, 3.9, and 3.6 Å) was similar to the β_T structure, but C18HPC exhibited a diffraction pattern close to the combination of α_H (4.2 Å) and β_T (4.5, 3.9, and 3.6 Å) packings. The complex diffraction pattern in C18HPC may suggest more than one mode of side-chain arrangement and may also account for the double melting in the DSC heating scan of the as-prepared sample. For C6HPC and C8HPC, the alkyl chains are also regularly arranged, as seen in Figure 6. However, the side chains do not show a separate T_s in the DSC experiments.

As described in the Introduction, the two alkyl side chains on the C2 and C3 positions are too close to accommodate another incoming alkyl chain. Instead of interdigitation, side-chain order in our polymers must arise from a different type of arrangement. One possibility is parallel arrangement of the tilted alkyl chains,[25] which was proposed in alkyl-substituted aromatic polyesters.[9,26] In support of this model, a computer simulation of poly(*p*-(2,5-di-*n*-alkyl)phenylene)s suggested that side-chain order was plausible when *n* was greater than 8 and the backbone repeating unit was more than 6, with a torsion angle of about 70°.[27] The semiflexible nature of the cellulose backbone of C*n*HPC's more likely allows conformational adjustments to be made so that side-chain ordering is facilitated.

(b) Effect of Thermal History on Side-Chain Crystallinity. Side-chain crystallinity in C12HPC and C18HPC, as manifested by DSC and X-ray results, was found to be highly dependent on the thermal history of the specimens. In the following, the symbol 18/M/-10 represents C18HPC cooled from the melt at a rate of 10 °C/min and 18/M/-20 the sample cooled at 20 °C/min. C18HPC and C12HPC quenched from the melt directly in liquid nitrogen are designated as 18/M/Q and 12/M/Q, respectively. The as-made polymers which have been annealed at 65 °C followed by 1, 10, and 20 °C/min cooling are denoted as 18/A/-1 and so on. All the samples were reheated at a rate of 10 °C/min from the subambient in the DSC experiments. The T_s, ΔH_s, T_i, and ΔH_i values of these polymers are listed in Table 3.

For C18HPC, the side-chain melting endotherms changed from the double-melting peak seen in the first heating scan of the as-made sample to a single peak when it was cooled from the melt at either 10 or 20 °C/min. The 18/M/-10 and 18/M/-20 samples showed little differences in T_s (56 vs 55 °C) and ΔH_s (51.4 vs 48.3 J/g). Compared to the as-made C18HPC, the ΔH_s values of the two control-cooled samples were about half the original values. These results are suggestive of reorganization of the alkyl side chains as the sample was cooled from the molten state. WAXS experiments support the above assumption. The diffraction peak at 4.4 Å together with a shoulder at 4.5 Å, which were only seen in the as-made C18HPC, disappeared in the 18/M/-10 sample. Instead, the specimen displayed a weak diffraction at 3.7 Å in addition to the previously observed 4.2- and 3.9-Å peaks.

For as-made C18HPC, the annealing time at 65 °C was found to have little or no effect on ΔH_s and T_s as long as it exceeded 1 h. The 18/A/-1 and 18/A/-10 specimens had nearly the same T_s's (60 and 59 °C) and similar ΔH_s's (75.8 and 71.3 J/g); both were greater than the respective values of the samples cooled from the melt. In comparing the M- and A-series samples cooled at the same rates but from different initial temperatures (e.g. 18/M/-10 vs 18/A/-10), the smaller ΔH_s values of the M-series samples indicated that although the main-chain alignment preceded side-chain crystallization and limited the ordered packing of the alkyl groups, the latter process was improved by annealing at 65 °C. Evidence for better side-chain order in these annealed samples was manifested convincingly in two regards. First, the 18/A/-10 sample displayed a sharp melting endotherm at 59 °C which was not observed either in the as-made or the M-series specimens. Second, the WAXS profile of 18/A/-10 (Figure 8, top curve) exhibited a stronger diffraction at 4.3 Å.

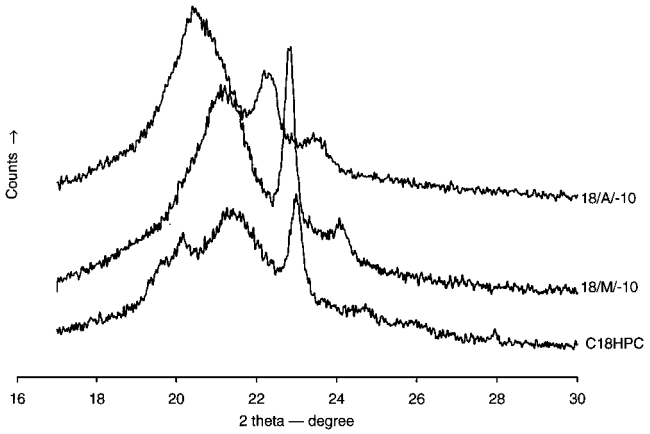

Figure 8. WAXS profiles of C18HPC thermally treated in different conditions.

Quenching the molten samples directly in liquid nitrogen also had a marked effect on the side-chain crystallinity. The side-chain melting endotherm became a relatively sharp peak at 38 °C which partially overlapped with a broad transition from 43 to 58 °C. However, the ΔH_s of the quenched C18HPC was slightly greater than those of 18/M/-10 and 18/M/-20. The slightly larger ΔH_s but smaller ΔH_i than other M-series samples appeared logical, since in this case the main-chain alignment was less perfect during quenching and exerted less constraint on order development of the side chains.

C12HPC showed no endotherm around 50 °C in the second scan after the sample was control-cooled from the melt, but the endotherm was clearly seen in the quenched sample which showed a larger ΔH_s but a lower T_s than those of the as-made sample. Interestingly, the large ΔH_s of the quenched sample was again accompanied by a smaller ΔH_i, as in 18/M/Q, but the results here are more clear-cut. We also noticed that although the magnitude of ΔH_s was high in the quenched sample, the melting transition was broad and T_s was low (only 36 °C). This observation was attributed to a broad distribution of less perfect crystals found in the quenching process.

(c) Effect of Side-Chain Organization on Main-Chain Packing. We have already mentioned that main-chain rigidity played an important role in the development of side-chain crystallinity. The backbones of the flexible polymers, on the other hand, had comparatively little impact on the development of side-chain order.[5] In a semiflexible polymer system such as C*n*HPC's, we have discussed in the preceding paragraphs the effect of main-chain alignment on side-chain order. Our next question is whether side-chain order may in turn influence the packing of the main chain. The question was answered in part by annealing experiments.

As we examined the effects of annealing at 65 °C on the ΔH_s and ΔH_i values of the as-made samples, we found that ΔH_i decreased but ΔH_s increased in C18HPC. Note that for all the A-series samples, the annealing temperature of 65 °C was far below the isotropization temperatures and presumably should have little effect on main-chain packing. Yet all the ΔH_i values were slightly smaller than those of the as-made sample. The smaller ΔH_i value was most noticeable for the 18/A/-1 sample. Annealing at 65 °C apparently not only led to side-chain reorganization upon subsequent slow cooling but also influenced main-chain alignment. We then

annealed the 18/M/-10 sample at 65 °C in the same way as 18/A/-10 and compared the results. Similar ΔH_i and ΔH_s values were obtained for the two, suggesting that the reorganization of alkyl side chains induced changes in main-chain packing regardless of the origins of the sample. In the C12HPC series, side-chain reorganization is also seen to have influenced the main-chain alignment when the results of 12/A/-1 and the as-made sample are compared.

A comparison of the data for the as-made and the three A-series samples already led to the suggestion that slow cooling from the annealing temperature, but not the annealing process itself, was responsible for the smaller ΔH_i value obtained for 18/A/-1. In order to substantiate this analysis, an additional DSC experiment was devised. The as-made C18HPC was annealed at 65 °C and then immediately heated, without first being cooled to room temperature, to the isotropic state. There was essentially no change in the ΔH_i value. The result supports the suggestion that the process of side-chain crystallization, but not conditioning at 65 °C by itself, affects backbone organization under certain conditions.

(d) Effect of Shear on Side-Chain Crystallization. We had illustrated the importance of thermal history on the packing of alkyl side chains. Another factor that influences chain alignment is mechanical shear. The effect of shear on side chain crystallization is shown in Figure 5. The side-chain melting endotherm of C12HPC, which was absent in the second heating scan of the as-made sample, reappeared in the sheared sample. Shearing also induced changes in the DSC results of C18HPC. In the split melting peaks at 57 and 37 °C, the former had a much higher enthalpy ($\Delta H_{57}/\Delta H_{37} \approx 3/1$). This is to be contrasted with the results for the as-made C18HPC in which the enthalpy ratio of the double-melting $\Delta H_{58}/\Delta H_{52}$ peaks was only about 0.6/1.

To explore the relation between the DSC melting endotherms and the structure changes in the sheared samples, WAXS experiments were conducted. The diffraction profile of the sheared C12HPC clearly showed that peaks in the wide-angle region had been reinforced. We would like to think that the reinforced peaks are related to the melting peak at 45 °C in the DSC scan. The effect of shear was clearer in the WAXS diffraction of C18HPC (Figure 7a). The sheared specimen displayed strong diffractions at 4.2 and 3.9 Å, and the relative intensity of 4.2/3.9 Å was apparently enhanced. The enhanced diffraction at 4.2 Å (α_H) correlated with the DSC result which revealed a greater magnitude in ΔH_{57}. However, if the effect of shear was eliminated by conditioning the sample in the molten state, in accordance with process 2, the intensity of diffraction at 3.9 Å decreased markedly in C12HPC (Figure 7b) and declined also in C18HPC. At the same time, the removal of the shear caused the disappearance of the low-temperature melting endotherm of C12HPC and brought the split peaks of C18HPC back to a single peak at 56 °C. The DSC and WAXS experiments thus clearly demonstrate the effect on packing and the reorganization of alkyl chains induced by shear.

Conclusions

A series of alkyl-substituted semiflexible polymers were synthesized by reacting hydroxypropylcellulose with hexyl, octyl, dodecyl, and octadecyl isocyanates. Side-chain crystallization was observed in C12HPC and C18HPC. The degree of side-chain crystallinity was found to be dependent on the thermal history and the application of shear. Reorganization of alkyl side chains was realized as the samples underwent thermal transitions. Due to the semiflexible nature of the cellulose backbone, reorganization of the alkyl side chains could result in a change in the main-chain packing induced by annealing the sample above T_s but below T_i, followed by very slow cooling to room temperature. The competition between the side chains and the backbone on morphological development was discussed.

Acknowledgment. We gratefully acknowledge the support of this investigation by the National Science Foundation, Division of Materials Research, Grants 9201003 and 9424317. Acknowledgment is also made to the donors of the Petroleum Research Fund, administered by the American Chemical Society, for support of this study. Thanks are also due to TA Instruments for providing the modulated calorimetric instrument for this research.

References and Notes

(1) Jones, A. T. *Makromol. Chem.* **1964**, *71*, 1.
(2) Jordan, E. F.; Feldeisen, D. W.; Wrigley, A. N. *J. Polym. Sci. A-1* **1971**, *9*, 1835.
(3) Jordan, E. F. *J. Polym. Sci., Polym. Chem.* **1972**, *10*, 3347.
(4) Platé, N. A.; Shibaev, V. P.; Petrukhin, B. S.; Zubov, Y. A.; Kargin, V. A. *J. Polym. Sci. A-1* **1971**, *9*, 2291.
(5) Morawetz, H.; Hsieh, H. W. S.; Post, B. *J. Polym. Sci., Polym. Phys.* **1976**, *14*, 1241.
(6) Majnusz, J.; Catala, J. M.; Lenz, R. W. *Eur. Polym. J.* **1983**, *19* (10/11), 1043.
(7) Ballauff, M.; Schmidt, G. F. *Mol. Cryst. Liq. Cryst.* **1987**, *147*, 163.
(8) Duran, R.; Ballauff, M.; Wenzel, M.; Wegner, G. *Macromolecules* **1988**, *21*, 2897.
(9) Rodriguezz-Parada, J. M.; Duran, R.; Wegner, G. *Maacromolecules* **1989**, *22*, 2507.
(10) Kricheldorff, J. H.; Domschke, A. *Macromolecules* **1996**, *29*, 1337.
(11) Berger, K.; Ballauff, M. *Mol. Cryst. Liq. Cryst. Inc. Nonlin. Opt.* **1988**, *157*, 109.
(12) Steuer, M.; Horth, M.; Ballauff, M. *J. Polym. Sci., Polym. Chem.* **1993**, *31*, 1609.
(13) Kricheldorff, J. H.; Domschke, A. *Macromolecules* **1994**, *27*, 1509.
(14) Wendorff, J. H.; Hermann-Schonherr, O. *Makromol. Chem. Rapid Commun.* **1986**, *7*, 791.
(15) Tashiro, K.; Ono, K.; Minagawa, Y.; Kobayashi, M.; Kawai, T.; Yoshino, K. *J. Polym. Sci., Polym. Phys.* **1991**, *29*, 1223.
(16) Chen, S.-A.; Ni, J.-M. *Macromolecules* **1992**, *23*, 6081.
(17) Hsu, W.-P.; Levon, K.; Ho, K.-S.; Myerson, A.; Kwei, T. K. *Macromolecules* **1993**, *26*, 1318.
(18) Zheng, W.-Y.; Levon, K.; Laakso, J.; Osterholm, J.-E. *Macromolecules* **1994**, *27*, 7554.
(19) Lee, D.-S.; Perlin, A. S. *Carbohydr. Res.* **1982**, *106*, 1.
(20) Lee, H. S.; Wang, Y. K.; Macknight, W. J.; Hsu, S. L. *Macromolecules* **1988**, *21*, 270.
(21) Heberer, D.; Keller, A.; Percec, V. *J. Polym. Sci., Polym. Phys.* **1995**, *33*, 1887.
(22) Chang, S.; Han, C. D. *Macromolecules* **1996**, *29*, 2103.
(23) Broadhurst, M. G. *J. Res. Nat. Bur. Stand.* **1962**, *66A*, 241.
(24) Müller, A.; Lonsdale, K. *Acta Crystallogr.* **1948**, *1*, 129.
(25) Lee, J. L.; Pearce, E. M.; Kwei, T. K. *Macromolecules*, in press.
(26) Stern, R.; Ballauff, M.; Lieser, G.; Wegner, G. *Polymer* **1991**, *32* (11), 2096.
(27) Park, K. C.; Dodd, L. R.; Levon, K.; Kwei, T. K. *Macromolecules* **1996**, *29*, 7149.

MA970404K